Chemical Engineering Journal 412 (2021) 128649

Contents lists available at ScienceDirect

Chemical Engineering Journal

journal homepage: www.elsevier.com/locate/cej

Wide linear range and highly sensitive flexible pressure sensor based on multistage sensing process for health monitoring and human-machine interfaces

Mengjuan Zhong [a,1], Lijuan Zhang [a,1], Xu Liu [a], Yaning Zhou [a], Maoyi Zhang [b,c], Yangjian Wang [a], Lu Yang [a], Di Wei [a,*]

[a] Beijing Graphene Institute, Beijing 100094, China
[b] State Key Laboratory of Nonlinear Mechanics, Institute of Mechanics, Chinese Academy of Sciences, Beijing 100190, China
[c] School of Engineering Science, University of Chinese Academy of Sciences, Beijing 100049, China

ARTICLE INFO

Keywords:
Linear sensitivity
Wide range
Micro-patterns
Flexible pressure sensor
Human-machine interface

ABSTRACT

Flexible pressure sensors have promising applications in wearable electronic devices. However, fabricating flexible pressure sensors with wide linear range and high sensitivity remain a great challenge. Herein, a micro-nano hybrid conductive elastomer film based on carbon materials with arched micro-patterns array on surface (P-HCF) is developed to show expected sensing properties through a sustainable route. The 1D carbon fibers (CFs) and 0D carbon nanoparticles (CNPs) were incorporated into polydimethylsiloxane (PDMS) matrix to construct a 3D conductive network consisting of physical contact and tunneling effect among carbon materials to improve the sensing range and sensitivity. The arched micro-patterns of the P-HCF, which is designed mimicking the human fingerprints, influences the pressure distribution inside the material, giving rise to a linear sensitivity over the whole sensing range. Finite element analysis (FEA) method is investigated to simulate and analyze the compression process. The P-HCF sensor exhibits both a high sensitivity of 26.6 kPa^{-1} and an exceptionally wide linear range of 20 Pa – 600 kPa. The devices were demonstrated in monitoring artery pulses, assisting in diagnosing Parkinson's disease, and analyzing gait for healthcare. Furthermore, the sensors are integrated into complex devices to realize pressure distribution detection, controlling manipulator, and operating PC games. The attainment of excellent pressure sensing performance of the P-HCF, potentially initiates vast applications in health monitoring and human-machine interfaces.

1. Introduction

Rapid advances in materials, flexible sensors, energy storage devices, and integrated systems are driving great interests in wearable electronic devices, which enable real-time monitoring and diagnosing of personal health status [1–4]. Flexible pressure-sensitive devices have drawn sustainable attention on prosthesis, health monitoring, and robotics [5–7]. The flexible pressure sensors could be classified into resistive [8,9], capacitive [10,11], piezoelectric [12,13] and optical [14,15] types, based on different sensing elements and mechanisms. Among these types of pressure sensors, resistive-type pressure sensors transducing mechanical features into resistance changes are extremely desirable due to their simple read-out mechanisms and cost effectiveness [16].

In the current study, most research carried out on expanding sensing range and improving sensitivity to satisfy the requirements of practical applications. Some effective methods were utilized to increase the sensing pressure or sensitivity including new materials and structural modifications. For example, our previous work had exhibited an ultra-wide sensing range up to 800 kPa via synthesizing micro-nano hybrid-structured conductive elastomer sensing film [17], and Sun *et al.* reported a conductive graphite/polydimethylsiloxane (G/PDMS) foam film with hierarchical surface microstructures to obtain an extremely high sensitivity of 245 kPa^{-1} [18]. Several materials with the outstanding properties were investigated in pressure sensors, such as conductive polymers [19], graphite [20], carbon nanotubes (CNTs) [21-

* Corresponding author.
E-mail address: diwei@hotmail.com (D. Wei).
[1] co-first author.

https://doi.org/10.1016/j.cej.2021.128649
Received 30 September 2020; Received in revised form 17 December 2020; Accepted 18 January 2021
Available online 23 January 2021
1385-8947/© 2021 Published by Elsevier B.V.

23], grapheme [24], carbon nanofibers (CFs) [25] and other nanomaterials [26,27]. Another way to improve sensing performance was through designing surface structures such as shapes of microdomes, micropyramids and other microstructures on surface or make micropores inside materials at the micro or even nano-scale [28–32]. However, under high pressure loading, materials' compressibility reduces, thus the number of conductive paths in pressure-resistive devices and the contact area of the contact-type devices become saturated, resulting in a decreased sensitivity and nonlinear response [33]. Therefore, with regard to flexible sensors, it is difficult to keep a satisfied sensitivity at high pressure region.

The linear sensitivity of sensor is the relationship between the output signals and the applied loads. In practical applications, the pressure sensors need to be operated in a linearity sensitive regime, which is instructive in avoiding additional signal processing for cost effectiveness and obtaining accurate information [5,33,34]. Besides the flexible pressure sensors could match existing signal processing systems on the market directly and show better market prospects in artificial intelligence, health care and other fields. However, few articles have reported the sensors with linear sensitivity in the whole sensing range. Researchers are continuously taking more efforts to improve the linear sensing range and sensitivity. For instance, Cho *et al.* [5] showed a pressure-sensitive electronic skin based on reduced graphene oxide (rGO) covering on PDMS microdome structure array with a sensitivity of 8.5 kPa^{-1} between 0 and 12 kPa. The sensing range belonged to the very low-pressure regime for just monitoring gentle touch. Wong *et al.* [6] conversed rigid nonconductive bulk wood trunks into flexible and conductive carbon/silicon composites as sensing material showing a sensitivity of 10.7 kPa^{-1} in wide pressure region (up to 100 kPa). Recently, Yang *et al.* [35] reported a novel pressure sensor with hierarchical microstructures presenting a higher sensitivity of 15.4 kPa^{-1} in a broad linearity range over 200 kPa. Although correlational research has obtained preferable results, it is still difficult to meet the requirements of real applications at high pressure range. In order to broaden the application scenarios, how to enlarge linear sensing range continuously while ensuring high sensitivity is a critical challenge.

In this paper, we presented a high-performance P-HCF flexible pressure sensor with an outstanding linear sensitivity of 26.6 kPa^{-1} over exceptionally wide pressure range from 20 Pa to 600 kPa, based on a multistage sensing process. Different from the majority flexible sensors, which depended on the modification of surface structures to obtain linear sensitivities, this sensing materials was not only designed to establish micro-nano hybrid-structure by using multi-dimensional carbon materials in the P-HCF in the micro-scale, but also had arched micro-patterns array mimicking the structure of human fingerprint on the surface in macro-scale for realizing multistage sensing. The compression process of sensor was simulated by finite element analysis (FEA) method. Attributed to the change in contact resistance of micro-patterns with the synergistic effect of physical contact among conductive fillers and tunneling effect inside the conductive elastomer, with the increases in the pressure, the high linear sensitivity maintained through the whole pressure range. Owing to these excellent properties, the sensors manifested outstanding performances with tremendous applications potential, such as human physiological signal monitoring, pressure distribution, and human-machine interfaces including controlling manipulator and playing games.

2. Experimental section

2.1. Preparation of P-HCF and pressure sensor

The P-HCF was fabricated by molding the liquid mixture of conductive elastomers on templates. CFs (diameter: 8 μm, length: 10–100 μm) (400 mesh, Haotian Nano Technology Company) and PDMS (Dow Corning Sylgard 184; the weight ratio of base to curing agent was 10:1) were mixed by a planetary centrifugal mixer (Kurabo, KK-250S). Conductive carbon ink (CCI, JUJO CHEMICAL Co., Ltd) were then added into CFs/PDMS and stirred by an overhead stirrer (IKA, RW20) at 400 rpm for 3 h. The conductive elastomer was bladed onto patterned quartz templates, which were engraved by laser flash (Speedy 360, 60 W) based on programmable patterning with different spacings and depths. The spacings of micro-patterns were 200 μm, 300 μm, and 400 μm; and the depths were 25 μm, 55 μm, 80 μm and 110 μm. Then after degassing in vacuum oven and fully curing under 100 °C, the micro-patterned HCFs with a bulk film thickness of ~ 500 μm were peeled off from templates. The as prepared P-HCF was cut into square size (1 × 1 cm) to be used as a sensing layer of pressure sensor to measure the sensing performance. The square P-HCF, which was hold the patterned side up, was fixed on the lower copper-clad laminate electrode by conductive silver adhesives. And the upper copper electrode was fixed on the linear motor, which can move along z-axis and ensure that the pressure sensor starts from off-state.

2.2. Characterization of thin films and pressure sensors

The morphologies of micro-patterned HCFs were characterized by SEM (10 kV, FEI Quattro S) with a 10.0 kV accelerating voltage and 3D profile (Sensofor). A mechanical performance testing system (MTS E43.104) was used to apply the pressure and a digital source meter (Keysight B2902A) was investigated to record the electrical responses of the sensors. The applied voltage for measurements of all electrical properties was 0.05 V DC. The curves of pulse monitoring, pressure array, gait monitoring, objects grabbing and gesture recognition demonstrations were acquired by source meter and electrochemical workstation (Metrohm, M204), respectively.

2.3. FEA numerical modeling

ABAQUS FEA software package was used to study the uniaxial compression behavior of the P-HCF. In order to save computing resources, the 3 × 3 array models were established. The composite material was treated as hyperelastic material depicted by the Marlow model, and parameters were decided by uniaxial test data. The composite material was modeled by the hexahedron element (C3D8R). Displacement boundary conditions were applied in load module.

2.4. Fabrication of stretchable pressure sensor array

The 4 × 4 array of stretchable pressure sensor was fabricated starting from the lower circuit board that was made from single-side Cu-clad laminate consisting of 18 μm thick Cu sheet and 75 μm thick supporting PI. The fabrication began with patterning 300 μm wide Cu meanders and island-like electrodes of sensors (size: 1.4 × 1.4 cm) by photolithography and wet etching along with the design. A 12.5 μm thick protect layer was coated on the upside of Cu meanders. The island bridge-like outline was structured by laser cutting, and then the flexible printed circuit board (FPCB) residues were removed. The 4 "islands" were connected in series as a column. The upper circuit board was fabricated by the same process, with 4 "islands" connected in series as a row. The square P_{55}-HCF (size: 1.2 × 1.2 cm) was fixed on each "island" of the lower circuit board by coating the precursor of HCF between the square P_{55}-HCF and the electrode and curing at 100 °C. Then, the upper circuit board covered on the square P_{55}-HCF according to the outlines of the lower circuit board. The sides of the square P_{55}-HCF coated silicon glue for adhering the island-like electrode of the upper circuit board to be sandwich configuration of upper electrode/P_{55}-HCF/lower electrode as sensing unit. Meanwhile, the Cu meanders of the upper and lower of circuit boards were adhered by the silicon glue on the overlapping sections. The 4 × 4 array of stretchable pressure sensor with island bridge-like outline was fabricated. The "island" was the sensing unit, and the "bridge" acted as a wire to transmit signals while make the device stretchable." The signals were processed by the external processing module.

2.5. Fabrication of flexible smart insole

The flexible smart insole was designed to lay out 16 sensing units placed at toes (#1–3), fore-foot (34–8), lateral (#9), and rear-foot (#10–16). The fabrication started from the lower circuit board printed the conductive silver paste on the PET film by screen printing technique. These rectangular (length: 23 mm, width: 11.5 mm) areas were used as the lower electrode of the sensing units, and connected by silver wires (width: 500 μm) in series as a row. The as-prepared P_{55}-HCF was fixed on each lower electrode by coating the precursor of HCF between the P_{55}-HCF and the electrode and curing at 100 °C. Then, the upper circuit board was printed the silver-based circuit by screen printing technique, including rectangular areas as the upper electrodes of the sensing units and connecting wires in series as a column. The upper and lower circuit boards overlapped face to face, and were adhered by silicon tape to be the flexible smart insole. The transmitting signals were collected and processed by an external processing module.

2.6. Fabrication of smart glove

The smart glove consists of commercial gloves and sensing device which was fixed on the back of the glove by covering thermoplastic tape. Five pressure sensors of the sensing device were set on the knuckles, respectively, and the signals were transmitted by Cu meanders to the signal processing module installed on the wrist. The substrate circuit that included electrodes of sensors and Cu meanders was made from flexible double-sided Cu-clad laminate consisting of 18 μm thick Cu sheet and 75 μm thick supporting PI. The 200 μm wide Cu meanders and the electrodes of sensor (length:22 mm, width:10 mm) were prepared by photolithography and wet etching along with the standard design. A 12.5 μm thick protect layer was coated on the upside of Cu meanders. The details of circuit configuration for each sensor and associated wire were descripted in the Fig. S8, showing that the upper and lower Cu meanders overlapped to reduce the width of wire. The upper electrode of sensor which connected to the end of lower Cu meander. The lower electrode of sensor that was prepared by FPCB process was welded to the bonding pad which was reserved at the end of upper Cu meander by drilling process. The as-prepared P_{55}-HCFs (length: 17 mm, width: 5 mm) were fixed on the lower electrodes by coating the precursor of HCF between the sensor material and the electrode and curing at 100 °C. A rectangular hollow double-sided tape was put on the sides of the P_{55}-HCF to adhere the upper and lower electrodes while maintained sensor off-state.

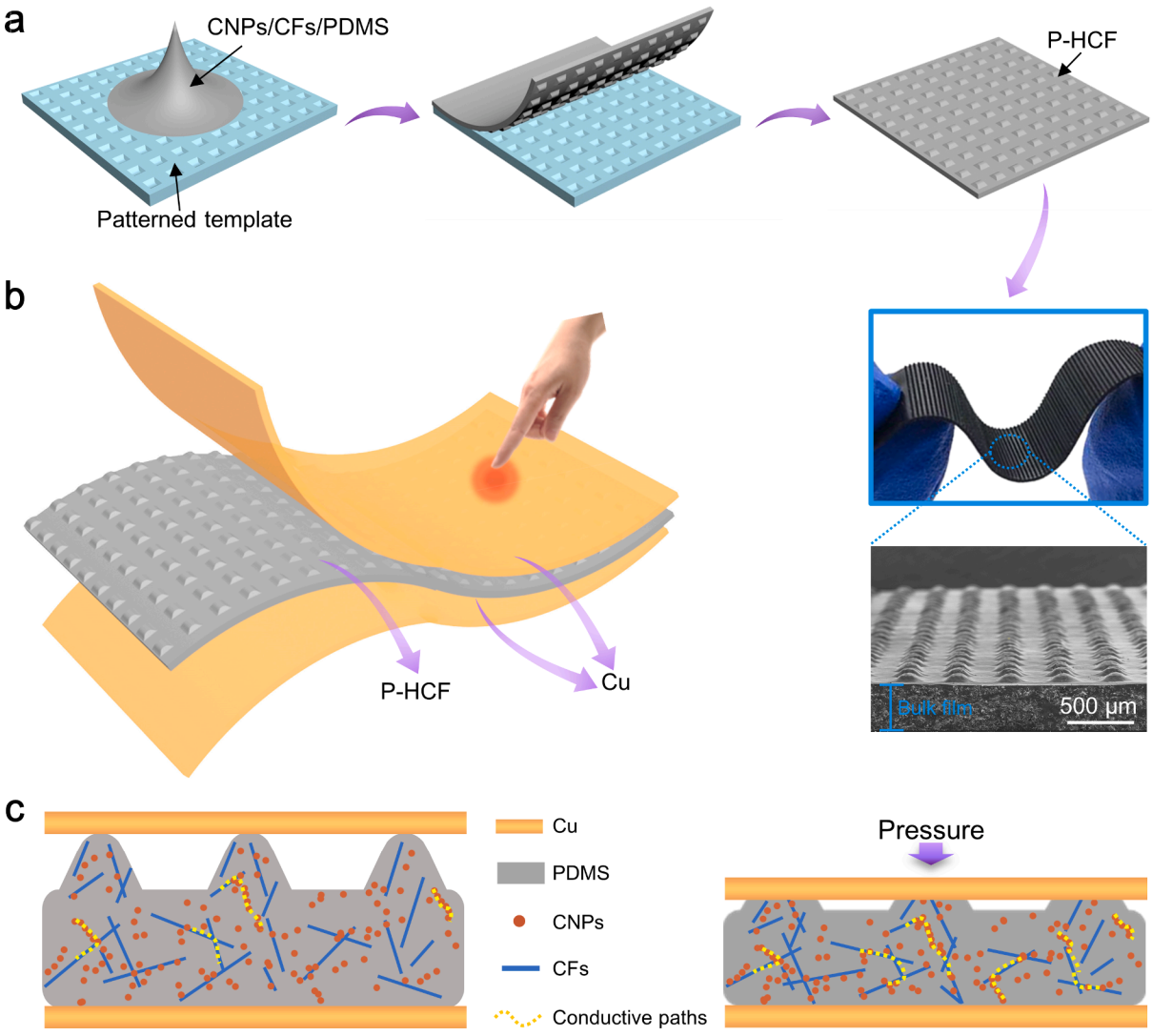

Fig. 1. A micro-nano hybrid carbon materials conductive elastomer film with arched micro-patterns array (P-HCF). (a) Schematic of the fabrication procedure of the P-HCF. (b) The configuration of flexible pressure sensor and the photo and SEM image of the P-HCF. (c) Schematic showing the basic working principle of the pressure sensor.

3. Results and discussion

The micro-nano hybrid carbon materials conductive elastomer film with arched micro-patterns array (P-HCF) is developed using a facile and sustainable route, the fabrication process of P-HCF is illustrated in Fig. 1a. The P-HCF was prepared by molding the liquid blending of conductive elastomers, which was synthesized by 1D CFs, 0D CNPs coming from conductive carbon ink and PDMS with the method reported in previous work [17], the details were listed in experimental section. The liquid blending of conductive elastomer was doctor bladed onto the patterned quartz templates, which were engraved by laser flash based on programmable patterning with different spacing and depths. The laser engraving method is superior to traditional lithography technique that is expensive and time-consuming. After degassing in vacuum oven and fully curing under 100 °C, the P-HCF with a bulk film thickness around 500 μm was peeled off from templates.

Fig. 1b presents the configuration of the flexible pressure sensor device. The P-HCF was sandwiched between two copper electrodes made of copper-clad laminates. Fig. 1c schematically shows the basic working principle of the pressure sensors. The external pressure changed the contact area between the micro-patterns array on the surface and the upper electrode, leading to the decrease in contact resistance. Meanwhile, the distance between CFs and CNPs inside P-HCF reduced, resulting on a sharp increase in conductive paths consisting of the physical contact and tunneling effect. Correspondingly, the total current of P-HCF sensor rose with the increase in applied pressure. The combination of the micro-nano hybrid structure film composed of internal multi-dimensional carbon materials and the arched micro-patterns array conducted a multistage sensing mechanism in the high-performance pressure sensors.

To demonstrate the effect of the height of the arched microstructure on the sensitivity and linear range of the flexible pressure sensor, four P-HCFs with different pattern heights (25 μm, 55 μm, 80 μm, and 110 μm) were prepared while keeping the pattern spacing and size at 200 μm, named as P_{25}-HCF, P_{55}-HCF, P_{80}-HCF, and P_{110}-HCF (Fig. 2a). Fig. 2b displays the 3D surface profiles of the P-HCFs, confirming that the surface micro-patterns array obtained by the laser engraved templates have uniform height and ordered distribution. Fig. 2c presents the sensing performance of flexible pressure sensors under applied pressures. The sensitivity (S) of the pressure sensors is defined as $S = (\Delta I/I_0)/\Delta P$, where ΔI and ΔP are the measured change in current and pressure, I_0 represents the initial current without loading. As a result, with the height of the surface pattern increasing, the normalized change in current ($\Delta I/I_0$) was gradually approached linear to applied pressure over entire 20 Pa − 600

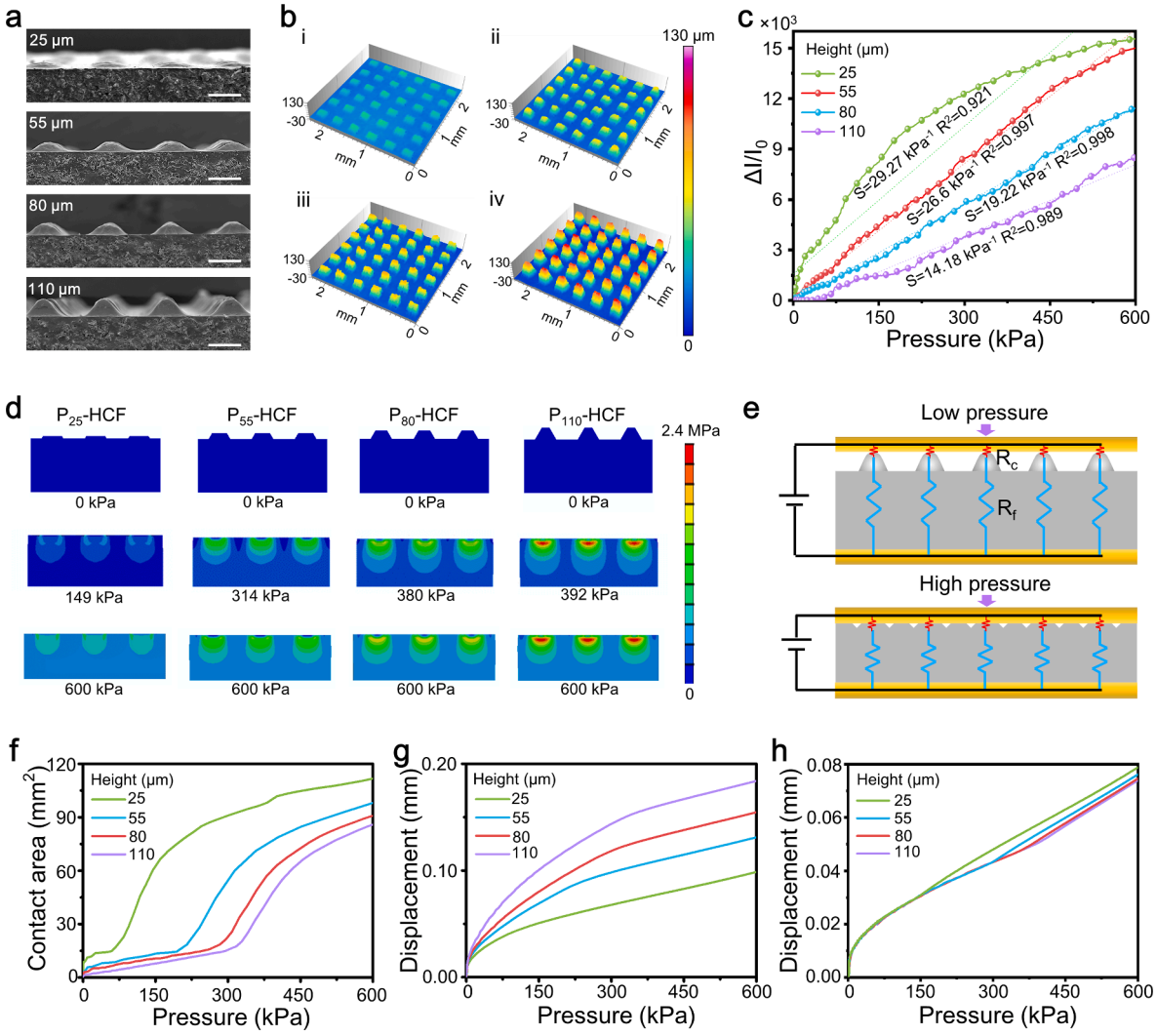

Fig. 2. Characterizations of the P-HCF sensors with different heights of micro-patterns. (a) SEM cross-section images (scale: 200 μm). (b) 3D surface profiles of HCFs (i: P_{25}-HCF, ii: P_{55}-HCF, iii: P_{80}-HCF, iv: P_{110}-HCF). (c) Current responses of the sensor to continuous pressure from 20 Pa to 600 kPa. (d) The stress distribution of the cross-section model obtained by FEA with the increase of applied pressure. (e) Circuit diagram of the P-HCF sensor. Change of contact area (f), total deformation (g) and deformation of bulk films (h) of P-HCFs in response to the applied pressure in FEA modeling.

kPa. At the same time, the sensitivity decreased from 29.27 to 14.18 kPa^{-1}, the highest linear sensitivity of 26.6 kPa^{-1} was achieved as the pattern height was 55 μm. The statistical data with errors was exhibited in the Fig. S1, and the standard deviation were all less than 5%.

To elucidate the effect of surface micro-patterns on sensor performances, FEA based on the model with different pattern heights was constructed to simulate the stress distribution and deformation process of the P-HCFs (Fig. S2 and S3). In the initial status, only the top surfaces of the patterns contacted with the upper electrode. Since the modulus of micro-patterns was lower than bulk film, the compression deformation of the micro-patterns was more than the bulk film. With the increase of the pressure, the micro-patterns were gradually flattened, at the same time, different heights of patterns required different pressures for flattening (P_{25}-HCF: 149 kPa, P_{55}-HCF: 314 kPa, P_{80}-HCF: 380 kPa, P_{110}-HCF: 392 kPa) (Fig. 2d). The pressure sensing mechanism of the P-HCF sensor consists of two parts of resistance changes (Fig. 2e): the contact resistance (R_c) and the film resistance (R_f). As shown in Fig. 2f, the contact area of the sensor gradually increased with increasing pressure. The sensing performance of the sensor started form the change in R_c caused by the increase in contact area at lower pressure, the greater the change in contact area, the higher the sensitivity of sensor [35–37]. As the pressure load is continuously applied, the change of R_f, which came from the tunneling and contact effects between inner conductive fillers resulting from the deformation of the pattern and bulk, gradually increased and synergized the R_c to act on the sensitivity of sensor [17,38,39]. Until patterns flattening, the change in resistance mainly depend on the R_f caused by the compression deformation of the bulk film. Take the P_{55}-HCF as an example, the compression process of cross section was shown in Movie S1, illustrating that the mises stress plot contours was constantly changing with the pressure increase. Fig. 2g shows the compression of different height sensors with pressure changes. Along the increase in height of micro-patterns, the procedure of micro-patterns flatting lasted longer and the deformation in bulk film declined (Fig. 2h). Therefore, the sensitivity of P_{25}-HCF sensor decreased and tended to saturation at high pressure, and the sensors with other heights of micro-patterns exhibited approximate linear sensitivity at the whole sensing range, as shown in Fig. 2c. Meanwhile, it can be seen that the P_{55}-HCF sensor showed higher linear sensitivity at the range of 20 Pa − 600 kPa. It could be summarized that the conductive materials can compensate for the saturation effect of the contact when the pressure becomes higher under reasonable design of micro-patterns to obtain a wide linear sensing range [33]. The underlying mechanism may be that the combination of contact resistance and film resistance promotes the sensor to show an excellent sensing performance with wide-linear and high sensitivity over the board sensing range.

On the basis of the above, the effect of spacing between micro-patterns was evaluated working on sensing performances (Fig. S4). The statistical data with errors was exhibited in the Fig. S5, and the standard deviation were all less than 5%. The sensitivity increased with the increase spacing, but the linearity of sensitivity was declining in the sensing range. It is obvious that the spacing of the micro-patterns determined the pressure sensing performance when the size and height of micro-patterns are same. As the spacing increases, the compressibility of the pressure sensor increases due to the decrease of the effective Young's modulus of the micro-patterns under the same pressure. The micro-patterns deform more and result in a larger contact area, resulting in higher sensitivity [37]. However, the micro-patterns with relatively wide spacing was earlier flattened, and the sensitivity of sensor reduced at high pressure to loss the linearity in the whole sensing range. While the sensor with higher density micro-patterns exhibited linear sensitivity at the broad sensing range as the synergistic effect of the contact resistance and film resistance generated during the sensing process. Therefore, the P_{55}-HCF with spacing and size of 200 μm was finally determined as the optimal pressure sensing materials. Moreover, the design of arched micro-patterns on the P_{55}-HCF mimicking the papillary lines on the fingerprint surface. It is well known that the height and width of the papillary lines are 0.1–0.4 mm and 0.2–0.5 mm, respectively, and it could be inferred from the literature that the width and spacing of papillary lines are roughly same [40]. It follows that the ratio of height and spacing of the papillary lines on the fingerprint surface is in the range of 1/5–2/1. For P_{55}-HCF, the proportion between height and spacing of arched micro-patterns is about 1/4, which is within the ratio of papillary lines. Therefore, the P_{55}-HCF sensor obtains outstanding sensing performance.

The current–voltage (I-V) curves of the P_{55}-HCF sensor from −3 to 3 V investigated at various pressure levels showed an obvious linear relationship and steady responses, demonstrating stable Ohmic characteristics (Fig. 3a). As the increasing of the applied load, the resistance (slope of the curves) decreased correspondingly. Aiming to investigate the limit of detection of the sensor (LOD), the current response to pressure was measured by loading/unloading 0.2 g of weight, as depicted in Fig. 3b and Fig. S6, indicating that the sensor could detect subtle pressure variations as low as 20 Pa. The instant sensing response time (40 ms) and recovery time (20 ms) could be observed in the inset, confirming the sensor has a timely manner under an external pressure and is comparable to that of human skin [41]. Fig. 3c and Table S1 shows a comparison of the sensing performance of the P_{55}-HCF sensor with other linear pressure sensors reported in the previous literature, demonstrating the higher sensitivity and broad sensing range for the P_{55}-HCF sensor simultaneously. Currently, most resistive-type sensors exhibited a linear range below 100 kPa [5,31,33,36,42,43]. Only a few sensors show a wider linear range, but the sensitivity is below 16 kPa^{-1} [35,44,45]. Therefore, this resistive-type sensor with a linear sensing range of 20 Pa to 600 kPa and sensitivity of 26.6 kPa^{-1} has rarely reported. To investigate the real-time pressure sensing performance of the P_{55}-HCF sensor under different pressures, the relative current change of the sensor was measured under incremental pressure. Fig. 3d demonstrates that the sensor could realize a rapid and linearly current changes at the middle-pressure range. It is notable that the well linear correlation between responding signals and pressure levels when the pressure continues to increase into the high pressure range (100–600 kPa), as shown in the Fig. 3e. Fig. 3f exhibits that the current responses of the P_{55}-HCF sensor to constant pressure loading of 200 kPa with different compression frequencies of 0.355 Hz, 0.712 Hz, 1.413 Hz and 2.769 Hz had been conducted. Observably, the pressure sensor always responded repeatedly during different compression frequencies. In order to confirm the durability and stability of the actual application, the P_{55}-HCF sensor performed 5000 compressive loading/unloading tests at 200 kPa, and obtained the corresponding sensing response of the pressure sensor in real time. As shown in Fig. 3g, it is found that the sensing response had no significant degradation in current amplitude over 5000 cycles, which indicated the stability and repeatability of the P_{55}-HCF sensor in long-term use. Besides, the performance of sensors under high temperature was explored. Fig. S7 exhibits the current responses of the sensors from 20 °C to 100 °C. Through the sensitivity performance reduced by 16.5% in 100 °C, it still has better sensing performance. Therefore, the sensor solves the problem that most commercial flexible sensors (operating temperature is below 60 °C) could not bear high temperatures and expands the application scenarios of flexible sensors.

To evaluate the potential applications of the pressure sensor in the diagnosis of cardiovascular diseases, the sensor was attached onto the wrist to detect the arterial pulse in real time (Fig. 4a). Here, a pulse frequency of 70 beats/min was recorded, corresponding to the value of healthy adults. Due to the excellent sensitivity and high signal–noise ratio of the sensor, is below the representative arterial waveforms without any signal amplification and post-processing were clearly visible: percussion wave (P_1), tidal wave (P_2) and diastolic wave (P_3). Parkinson's disease (PD) is a common neurodegenerative disease in the middle-aged and elderly people, and muscle rigidity is one of the typical symptoms of Parkinson's patients. The usual manifestation is the resistance to passive movement that occurs in both flexors and extensors

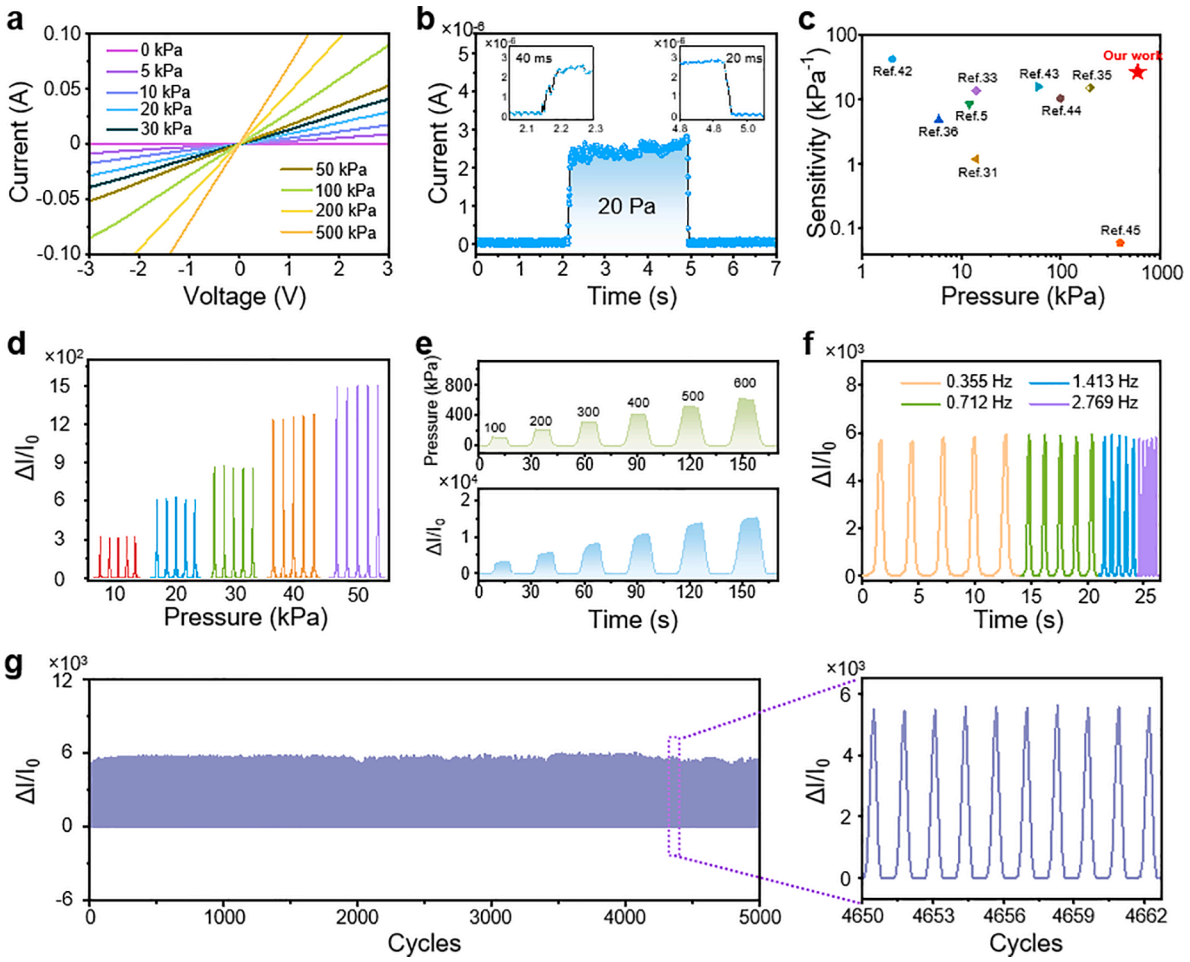

Fig. 3. Sensing performance of the P_{55}-HCF sensor. (a) The I-V curves of the sensor. (b) Current responses to loading/unloading 20 Pa on the sensor. Inserts were response time and recovery time of the sensor. (c) Comparison of linear sensing range and sensitivity between the P_{55}-HCF sensor with other reported sensors. (d) Cyclic current responses of the sensor to different pressures. (e) Real-time pressure monitoring of the P_{55}-HCF sensor at an applied pressure of 100, 200, 300, 400, 500, and 600 kPa. (f) Cyclic current responses of the sensor to 200 kPa at different frequencies. (g) Stability and durability of the sensor over 5000 loading/unloading cycles at a pressure of 200 kPa.

throughout the whole range of motion. Clinically, muscle rigidity is detected by passively moving an extremity at a joint [46]. Fig. 4b shows the sensor was attached onto the biceps to simulate the patient's muscle resistance during passive movement, and the corresponding current changes is shown in Fig. 4c, presenting that the P_{55}-HCF sensor could be well used for the diagnosis of Parkinson's disease. Besides, the flexible pressure sensors are integrated into sensing array to display the capability of intuitively perceiving the spatial distribution and value of pressure. Fig. 4d illustrates a 4 × 4 array of stretchable pressure sensor consisting of P_{55}-HCF sensors and stretchable circuit, which is conformal to the hemispherical mold due to its stretchability, manifesting that the stretchable sensing array could be conformal to complex surface in real applications. The value and location of the applied pressure from fingers and palm could be visualized by the height and position of 3D columnar mapping image (Fig. 4e - g), according to that, the distribution of pressure, or even rough outline of objects could be detected and recognized by the sensor array.

Monitoring of plantar pressure is of great significance to footwear design, injury prevention, sport biomechanicals and diagnosistic of foot diseases [47,48]. Practical plantar pressure monitoring requires wide-range linear sensing capability up to several hundreds of kPa and high sensitivity in order to achieve accurate information [49]. Here, a flexible smart insole consists of 16 sensing units placed at toes (#1–3), fore-foot (#4–8), lateral (#9) and rear-foot (#10–16) was developed to record foot pressure signals (Fig. 4h). Fig. 4i presents the pressure distribution of standing posture by a person with 50 kg mass. Benefit from the wide linear and high sensitivity of flexible sensors, pressure of each point could be collected accurately. Furthermore, the evolution of pressure mapping during dynamic walking was reconstructed from acquired data continuously received by 16 sensors. Plantar pressure distribution during walking process usually contains heel strike, foot flat, midstance, heel off and tiptoe strike, as shown in Fig. 4j. The intelligent insole could accurately record foot pressure distribution in real-time, where red parts indicated high pressure and blue parts represented relatively low pressure, and the pressure changed following the locomotion of emphasis. The evolution of plantar pressure experienced a highest stress in rear foot regime and nearly no stress in fore foot and toes for heel strike, transferred to stress localized in anterior region of fore foot and toes for tiptoe strike, which was in line with the real plantar pressure distribution during walking. The flexible smart sole is expected to be performed for early diagnosis Parkinson's disease or diabetic foot ulcers disease [50,51], resulted from excessive foot pressure and characteristic pressure distribution, providing abundant information for gait analysis, further giving suggestions in walking postures and foot health.

Human-machine interfaces enable the effective information interactions between people and machines, which play a crucial role in artificial intelligence, have been realized in various ways [52–54], such as wearable or implantable platforms integrated in watches, clothes, wrist bands, keyboards, and microphones, etc. Herein, a human–machine interface based on the flexible pressure sensors was

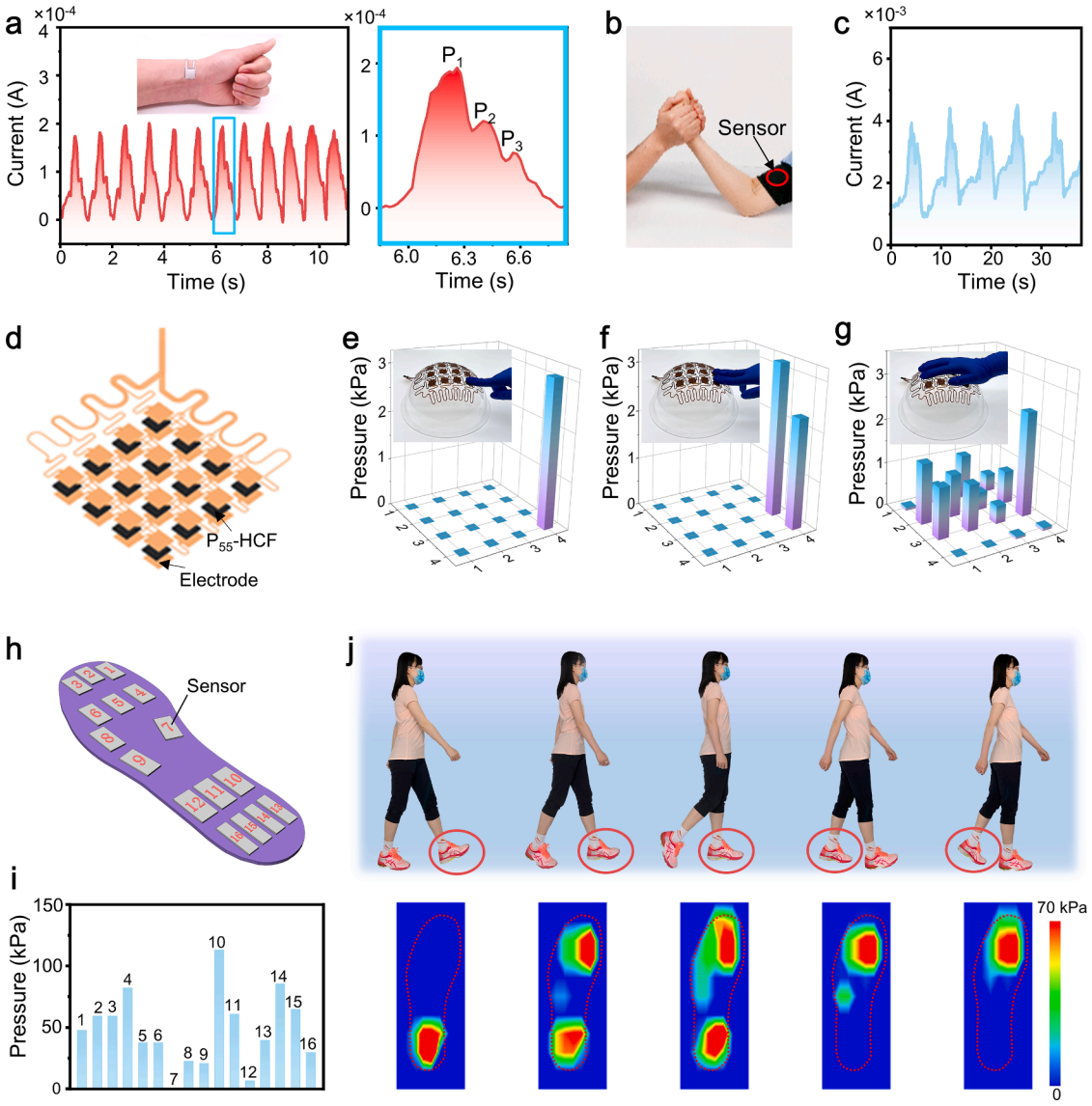

Fig. 4. Applications of the pressure sensors for health monitoring. (a) Flexible pressure sensor attached on the wrist for pulse signals monitoring. (b) and (c) attached on the biceps for simulating the patient's muscle resistance during exercise. (d) Schematic of the stretchable pressure sensor array assembled from the P_{55}-HCFs with 4 × 4 pixels. (e-g) Schematics of the fingers and palm touching on the pressure sensor array and corresponding pressure maps. (h) Schematic of the intelligent insole consisting of 16 pixels' sensors. (i) Plantar pressure distribution of left foot in standing posture. (j) Plantar pressure distribution during walking process measured by the intelligent insole.

established by affixing the sensing device to a textile glove at knuckle regions, as shown in Fig. 5a. The sensing device was fabricated by the upper and lower flexible circuits and the P_{55}-HCFs. The sensors were set to the knuckles with the sandwich configuration of Cu/ P_{55}-HCF/Cu. The Fig. S8 illustrates a sequential schematic diagram of the fabrication process. The upper and lower electrodes of sensors were from upper and lower flexible circuits, and the signals were transmitted by the Cu meanders. Moreover, the Cu meanders give the wires stretchability to avoid damage when the hand is moving. Details appear in the Experimental Section. Combined the on/off and amplitudes of five signals generated by fingers, the output curves could represent different gestures (Fig. 5b). In addition, the duration and frequency of signals might be defined as Morse code, which were controlled by the endurance and frequency of finger bending (Fig. 5c). Furthermore, the smart glove system recorded and processed the bending signals from each joint to operate the manipulator, such as gesture imitation (Fig. 5d, Movie S2) and grabbing object (Fig. 5e, Movie S3). And the current responses of different gestures were exhibited in Fig. S9. Apart from that, the smart glove also worked as a controller to build an intelligent rehabilitation training platform for patients (Fig. 5f). The functional commands of "running", "left", "jumping", "right", "boxing" were realized by bending thumb, index finger, middle finger, fourth finger and little finger, respectively (Fig. S10, Movie S4). The current responses of different command actions were shown in the Fig. S11. The intelligent rehabilitation training platform integrating data visualization, accurate training and entertaining could help patients to train and improve their finger joints skills though an interesting and challenging manner [55,56]. In view of the above, the flexible pressure sensor exhibited sufficient potential in human–machine interfaces and displayed potential application prospects in rehabilitation medical, as well as exoskeleton manipulator, or even industrial manufacturing.

4. Conclusion

In summary, we presented a flexible pressure sensor, which is from material synthesis to structure design. A high linear sensitivity at a wide

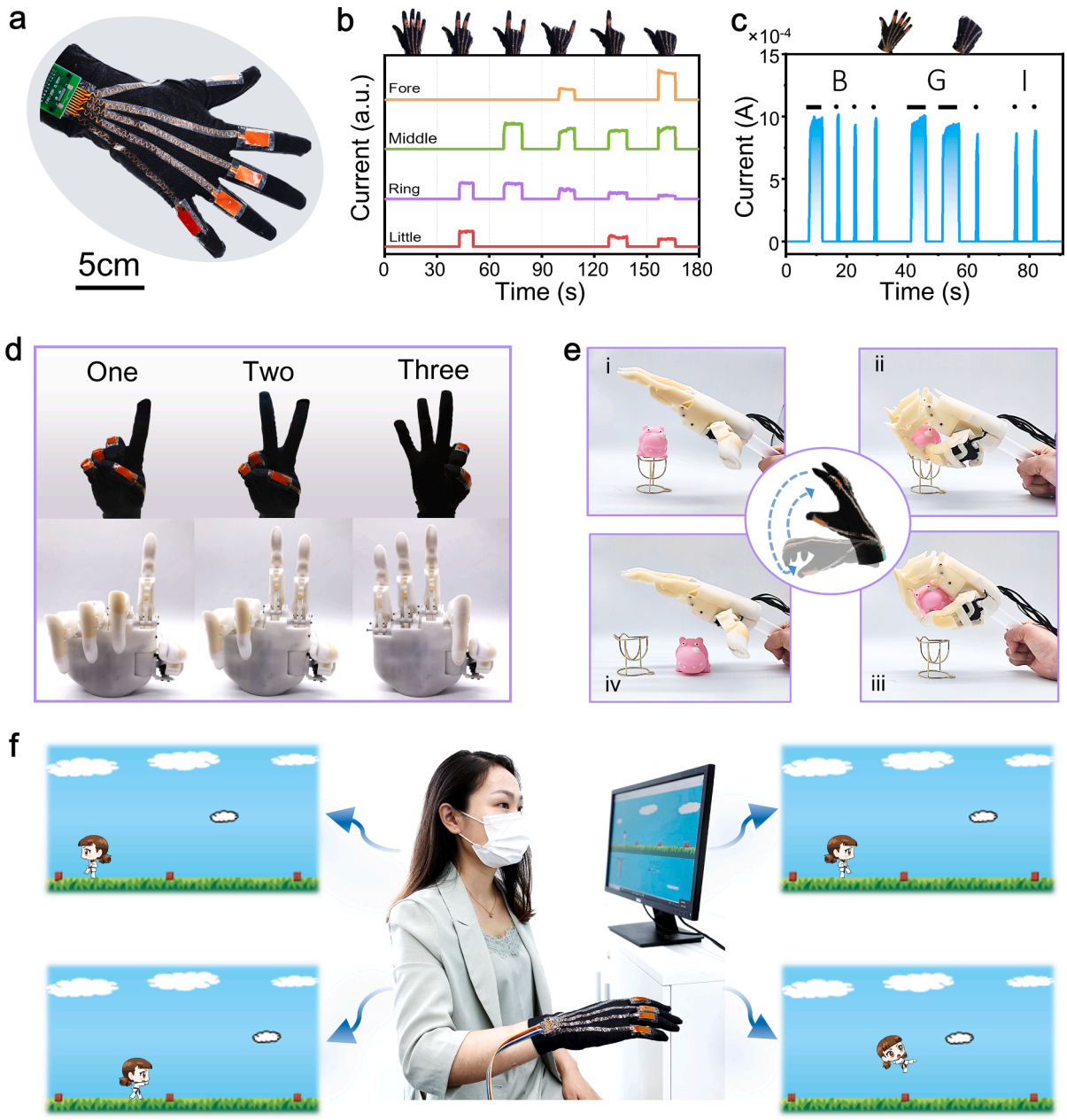

Fig. 5. Applications of the pressure sensors for human-machine interfaces and rehabilitation treatment. (a) Photography of the smart glove and schematic diagram of the control system. (b-c) Current responses of different gestures and Morse code for "BGI" produced by fingers bending. Images of controlling manipulator to (d) imitate gestures and (e) grab object. (f) The smart glove used in intelligent rehabilitation training through playing PC games.

sensing range through multistage sensing process could be realized. The sensing material P-HCF is fabricated by a simple and efficient approach to obtain the micro-nano hybrid-structured conductive film with arched micro-patterns array. 1D CFs and 0D CNPs as conductive fillers established 3D conductive networks in PDMS to become multistage sensing structure on micro-scale, greatly improved the sensing range and sensitivity of filler-matrix elastomer material. The micro-pattern array is designed on the surface mimicking the papillary lines on fingerprint surface to change pressure distribution to obtain linear sensitivity in whole sensing range. In addition, the sensors showed good sensing performance at 100 °C, in contrast most commercial flexible sensors could not withstand high temperatures, thus, it expands the application scenarios. The sensor is demonstrated in the detection of real-time arterial pulse signals, aided diagnosing Parkinson's disease, analyzing gait, perceiving pressure distribution, controlling manipulators, and operating PC games. These results reveal the significance of combining micro-patterns array of pressure-sensing materials with device design to realize flexible electronics for ubiquitous wearable applications, such as health monitoring, robot sensing and human–machine interfaces.

Declaration of Competing Interest

The authors declare that they have no known competing financial interests or personal relationships that could have appeared to influence the work reported in this paper.

Acknowledgements

This work was supported by Beijing Municipal Science & Technology Commission No. Z181100004818004, No. Z181100001018029, and No. Z191100006119027. The authors also appreciate the technical assistance from the BGI Characterization & Quality Assurance Center.

Appendix A. Supplementary data

Supplementary data to this article can be found online at https://doi.org/10.1016/j.cej.2021.128649.

References

[1] J.A. Rogers, X. Chen, X. Feng, Flexible hybrid electronics, Adv. Mater. 32 (15) (2020) 1905590.
[2] W. Shen, K. Li, Y. Lv, T. Xu, D. Wei, Z. Liu, Highly-safe and ultra-stable all-flexible gel polymer lithium ion batteries aiming for scalable applications, Adv. Energy Mater. 10 (2020) 1904281.
[3] K. Lee, X. Ni, J.Y. Lee, H. Arafa, D.J. Pe, S. Xu, R. Avila, M. Irie, J.H. Lee, R. L. Easterlin, D.H. Kim, H.U. Chung, O.O. Olabisi, S. Getaneh, E. Chung, M. Hill, J. Bell, H. Jang, C. Liu, J.B. Park, J. Kim, S.B. Kim, S. Mehta, M. Pharr, A. Tzavelis, J.T. Reeder, I. Huang, Y. Deng, Z. Xie, C.R. Davies, Y. Huang, J.A. Rogers, Mechano-acoustic sensing of physiological processes and body motions via a soft wireless device placed at the suprasternal notch, Nat. Biomed. Eng. 4 (2) (2020) 148–158.
[4] Y. Liu, J. Liu, S. Chen, T. Lei, Y. Kim, S. Niu, H. Wang, X. Wang, A.M. Foudeh, J.-H. Tok, Z. Bao, Soft and elastic hydrogel-based microelectronics for localized low-voltage neuromodulation, Nat. Biomed. Eng. 3 (1) (2019) 58–68.
[5] G.Y. Bae, S.W. Pak, D. Kim, G. Lee, D.H. Kim, Y. Chung, K. Cho, Linearly and highly pressure-sensitive electronic skin based on a bioinspired hierarchical structural array, Adv. Mater. 28 (26) (2016) 5300–5306.
[6] Z. Chen, H. Zhuo, Y. Hu, H. Lai, L. Liu, L. Zhong, X. Peng, Wood-derived lightweight and elastic carbon aerogel for pressure sensing and energy storage, Adv. Funct. Mater. 30 (2020) 1910292.
[7] Q. Zheng, J.-H. Lee, X.i. Shen, X. Chen, J.-K. Kim, Graphene-based wearable piezoresistive physical sensors, Mater. Today 36 (2020) 158–179.
[8] Z. Wang, X. Guan, H. Huang, H. Wang, W. Lin, Z. Peng, Full 3D printing of stretchable piezoresistive sensor with hierarchical porosity and multimodulus architecture, Adv. Funct. Mater. 29 (2019) 1807569.
[9] H.-B. Yao, J. Ge, C.-F. Wang, X.u. Wang, W. Hu, Z.-J. Zheng, Y. Ni, S.-H. Yu, A flexible and highly pressure-sensitive graphene-polyurethane sponge based on fractured microstructure design, Adv. Mater. 25 (46) (2013) 6692–6698.
[10] B.-K. Tee, A. Chortos, R.R. Dunn, G. Schwartz, E. Eason, Z. Bao, Tunable flexible pressure sensors using microstructured elastomer geometries for intuitive electronics, Adv. Funct. Mater. 24 (34) (2014) 5427–5434.
[11] G.Y. Bae, J.T. Han, G. Lee, S. Lee, S.W. Kim, S. Park, J. Kwon, S. Jung, K. Cho, Pressure/temperature sensing bimodal electronic skin with stimulus discriminability and linear sensitivity, Adv. Mater. 30 (2018), e1803388.
[12] X. Hou, S. Zhang, J. Yu, M. Cui, J. He, L. Li, X. Wang, X. Chou, Flexible piezoelectric nanofibers/polydimethylsiloxane-based pressure sensor for self-powered human motion monitoring, Energy Technol. 8 (2020) 1901242.
[13] D.Y. Park, D.J. Joe, D.H. Kim, H. Park, J.H. Han, C.K. Jeong, H. Park, J.G. Park, B. Joung, K.J. Lee, Self-powered real-time arterial pulse monitoring using ultrathin epidermal piezoelectric sensors, Adv. Mater. Interfaces 29 (2017) 1702308.
[14] P.C. Hui, K. Shtyrkova, C. Zhou, X. Chen, J. Chodosh, C.H. Dohlman, E.I. Paschalis, Implantable self-aligning fiber-optic optomechanical devices for in vivo intraocular pressure-sensing in artificial cornea, J. Biophotonics. 13 (2020), e202000031.
[15] M. Runowski, P. Woźny, S. Lis, V. Lavín, I.R. Martín, Optical vacuum sensor based on lanthanide upconversion—luminescence thermometry as a tool for ultralow pressure sensing, Adv. Mater. Technol. 5 (2020) 1901091.
[16] L. Pan, A. Chortos, G. Yu, Y. Wang, S. Isaacson, R. Allen, Y. Shi, R. Dauskardt, Z. Bao, An ultra-sensitive resistive pressure sensor based on hollow-sphere microstructure induced elasticity in conducting polymer film, Nat. Commun. 5 (2014) 3002.
[17] L. Zhang, X. Liu, M. Zhong, Y. Zhou, Y. Wang, T. Yu, X. Xu, W. Shen, L. Yang, N. Liu, D. Wei, Z. Liu, Micro-nano hybrid-structured conductive film with ultrawide range pressure-sensitivity and bioelectrical acquirability for ubiquitous wearable applications, Appl. Mater. Today 20 (2020), 100651.
[18] Q.-J. Sun, X.-H. Zhao, Y. Zhou, C.-C. Yeung, W. Wu, S. Venkatesh, Z.-X. Xu, J. J. Wylie, W.-J. Li, V.A.L. Roy, Fingertip-skin-inspired highly sensitive and multifunctional sensor with hierarchically structured conductive graphite/polydimethylsiloxane foams, Adv. Funct. Mater. 29 (2019) 1808829.
[19] B. Lee, J.Y. Oh, H. Cho, C.W. Joo, H. Yoon, S. Jeong, E. Oh, J. Byun, H. Kim, S. Lee, J. Seo, C.W. Park, S. Choi, N.M. Park, S.Y. Kang, C.S. Hwang, S.D. Ahn, J.I. Lee, Y. Hong, Ultraflexible and transparent electroluminescent skin for real-time and super-resolution imaging of pressure distribution, Nat. Commun. 11 (2020) 663.
[20] Q.-J. Sun, J. Zhuang, S. Venkatesh, Y. Zhou, S.-T. Han, W. Wu, K.-W. Kong, W.-J. Li, X. Chen, R.K.Y. Li, V.A.L. Roy, Highly sensitive and ultrastable skin sensors for biopressure and bioforce measurements based on hierarchical microstructures, ACS Appl. Mater. Interfaces 10 (2018) 4086–4094.
[21] H. Chen, Z. Su, Y. Song, X. Cheng, X. Chen, B. Meng, Z. Song, D. Chen, H. Zhang, Omnidirectional bending and pressure sensor based on stretchable CNT-PU sponge, Adv. Funct. Mater. 27 (2017) 1604434.
[22] B. Liang, Z. Zhang, W. Chen, D. Lu, L. Yang, R. Yang, H. Zhu, Z. Tang, X. Gui, Direct patterning of carbon nanotube via stamp contact printing process for stretchable and sensitive sensing devices, Nano-Micro Letters 11 (2019) 92.
[23] B. Liang, W. Chen, Z. He, R. Yang, Z. Lin, H. Du, Y. Shang, A. Cao, Z. Tang, X. Gui, Highly sensitive, flexible MEMS based pressure sensor with photoresist insulation layer, Small 13 (2017) 1702422.
[24] X. Chen, F. Luo, M. Yuan, D. Xie, L. Shen, K. Zheng, Z. Wang, X. Li, L.Q. Tao, A dual-functional graphene-based self-alarm health-monitoring E-skin, Adv. Funct. Mater. 29 (2019) 1904706.
[25] W. Yang, N.-W. Li, S. Zhao, Z. Yuan, J. Wang, X. Du, B. Wang, R. Cao, X. Li, W. Xu, Z.L. Wang, C. Li, A breathable and screen-printed pressure sensor based on nanofiber membranes for electronic skins, Adv. Mater. Technol. 3 (2018) 1700241.
[26] H. Ding, Z. Xin, Y. Yang, Y. Luo, K. Xia, B. Wang, Y. Sun, J. Wang, Y. Zhang, H. Wu, S. Fan, L. Zhang, K. Liu, Ultrasensitive, low-voltage operational, and asymmetric ionic sensing hydrogel for multipurpose applications, Adv. Funct. Mater. 30 (2020) 1909616.
[27] M. Chen, W. Luo, Z. Xu, X. Zhang, B. Xie, G. Wang, M. Han, An ultrahigh resolution pressure sensor based on percolative metal nanoparticle arrays, Nat. Commun. 10 (2019) 4024.
[28] Y. Zhang, Y. Hu, P. Zhu, F. Han, Y. Zhu, R. Sun, C.P. Wong, Flexible and highly sensitive pressure sensor based on microdome-patterned PDMS forming with assistance of colloid self-assembly and replica technique for wearable electronics, ACS Appl. Mater. Interfaces 9 (2017) 35968–35976.
[29] G. Schwartz, B.C. Tee, J. Mei, A.L. Appleton, D.H. Kim, H. Wang, Z. Bao, Flexible polymer transistors with high pressure sensitivity for application in electronic skin and health monitoring, Nat. Commun. 4 (2013) 1859.
[30] Q. Wang, A. Xiao, Z. Shen, X.-H. Fan, Janus particles with tunable shapes prepared by asymmetric bottlebrush block copolymers, Polym. Chem. 10 (2019) 372–378.
[31] J. Shi, L. Wang, Z. Dai, L. Zhao, M. Du, H. Li, Y. Fang, Multiscale hierarchical design of a flexible piezoresistive pressure sensor with high sensitivity and wide linearity range, Small 14 (2018), e1800819.
[32] T. Wang, J. Li, Y. Zhang, F. Liu, B. Zhang, Y. Wang, R. Jiang, G. Zhang, R. Sun, C.-P. Wong, Highly ordered 3D porous graphene sponge for wearable piezoresistive pressure sensor applications, Chemistry 25 (2019) 6378–6384.
[33] Y. Shu, H. Tian, Y. Yang, C. Li, Y. Cui, W. Mi, Y. Li, Z. Wang, N. Deng, B. Peng, T. L. Ren, Surface-modified piezoresistive nanocomposite flexible pressure sensors with high sensitivity and wide linearity, Nanoscale 7 (2015) 8636–8644.
[34] J. He, P. Xiao, W. Lu, J. Shi, L. Zhang, Y. Liang, C. Pan, S.-W. Kuo, T. Chen, A universal high accuracy wearable pulse monitoring system via high sensitivity and large linearity graphene pressure sensor, Nano Energy 59 (2019) 422–433.
[35] Z. Li, B. Zhang, K. Li, T. Zhang, X. Yang, A wide linearity range and high sensitivity flexible pressure sensor with hierarchical microstructures via laser marking, J. Mater. Chem. C 8 (2020) 3088–3096.
[36] C.L. Choong, M.B. Shim, B.S. Lee, S. Jeon, D.S. Ko, T.H. Kang, J. Bae, S.H. Lee, K. E. Byun, J. Im, Y.J. Jeong, C.E. Park, J.J. Park, U.I. Chung, Highly stretchable resistive pressure sensors using a conductive elastomeric composite on a micropyramid array, Adv. Mater. 26 (2014) 3451–3458.
[37] C. Ma, D. Xu, Y.C. Huang, P. Wang, J. Huang, J. Zhou, W. Liu, S.T. Li, Y. Huang, X. Duan, Robust flexible pressure sensors made from conductive micropyramids for manipulation tasks, ACS Nano 14 (2020) 12866–12876.
[38] N.N. Jason, M.D. Ho, W. Cheng, Resistive electronic skin, J. Mater. Chem. C 5 (2017) 5845–5866.
[39] N. Hu, Y. Karube, M. Arai, T. Watanabe, C. Yan, Y. Li, Y. Liu, H. Fukunaga, Investigation on sensitivity of a polymer/carbon nanotube composite strain sensor, Carbon 48 (2010) 680–687.
[40] A. Homola, Detection of papillary line width by fingerprints, Master thesis (2011).
[41] W. Wu, X. Wen, Z.L. Wang, Taxel-addressable matrix of vertical-nanowire piezotronic transistors for active and adaptive tactile imaging, Science 340 (2013) 952–957.
[42] Y. He, L. Zhao, X. Wang, L. Liu, H. Liu, Microstructured hybrid nanocomposite flexible piezoresistive sensor and its sensitivity analysis by mechanical finite-element simulation, Nanotechnol. 31 (2020), 185502.
[43] N. Luo, Y. Huang, J. Liu, S.C. Chen, C.P. Wong, N. Zhao, Hollow-structured graphene-silicone-composite-based piezoresistive sensors: decoupled property tuning and bending reliability, Adv. Mater. 29 (2017) 1702675.
[44] Y. Huang, Y. Chen, X. Fan, N. Luo, S. Zhou, S.C. Chen, N. Zhao, C.P. Wong, Wood derived composites for high sensitivity and wide linear-range pressure sensing, Small (2018), e1801520.
[45] H. Chang, S. Kim, T.H. Kang, S.W. Lee, G.T. Yang, K.Y. Lee, H. Yi, Wearable piezoresistive sensors with ultrawide pressure range and circuit compatibility based on conductive-island-bridging nanonetworks, ACS Appl. Mater. Interfaces 11 (2019) 32291–32300.
[46] A. Colcher, T. Simuni, Clinical manifestations of parkinson's disease, Med. Clinics of North Am. 83 (1999) 327–347.
[47] X. Wu, Y. Khan, J. Ting, J. Zhu, S. Ono, X. Zhang, S. Du, J.W. Evans, C. Lu, A. C. Arias, Large-area fabrication of high-performance flexible and wearable pressure sensors, Adv. Electron. Mater. 6 (2020) 1901310.
[48] Y. Li, S. Luo, M.-C. Yang, R. Liang, C. Zeng, Poisson ratio and piezoresistive sensing: a new route to high-performance 3D flexible and stretchable sensors of multimodal sensing capability, Adv. Funct. Mater. 26 (2016) 2900–2908.
[49] Y. Lee, J. Park, S. Cho, Y.-E. Shin, H. Lee, J. Kim, J. Myoung, S. Cho, S. Kang, C. Baig, H. Ko, Flexible ferroelectric sensors with ultrahigh pressure sensitivity and linear response over exceptionally broad pressure range, ACS Nano 12 (2018) 4045–4054.
[50] C. Lou, S. Wang, T. Liang, C. Pang, L. Huang, M. Run, X. Liu, A graphene-based flexible pressure sensor with applications to plantar pressure measurement and gait analysis, Materials (Basel) 10 (2017) 1068.
[51] B. Nie, R. Huang, T. Yao, Y. Zhang, Y. Miao, C. Liu, J. Liu, X. Chen, Textile-based wireless pressure sensor array for human-interactive sensing, Adv. Funct. Mater. 29 (2019) 1808786.

[52] Q. He, Y. Wu, Z. Feng, C. Sun, W. Fan, Z. Zhou, K. Meng, E. Fan, J. Yang, Triboelectric vibration sensor for a human-machine interface built on ubiquitous surfaces, Nano Energy 59 (2019) 689–696.
[53] C.-Z. Hang, X.-F. Zhao, S.-Y. Xi, Y.-H. Shang, K.-P. Yuan, F. Yang, Q.-G. Wang, J.-C. Wang, D.W. Zhang, H.-L. Lu, Highly stretchable and self-healing strain sensors for motion detection in wireless human-machine interface, Nano Energy 76 (2020), 105064.
[54] M. Zhu, Z. Sun, Z. Zhang, Q. Shi, T. He, H. Liu, T. Chen, C. Lee, Haptic-feedback smart glove as a creative human-machine interface (HMI) for virtualaugmented reality applications, Sci. Adv. 6 (2020) eaaz8693.
[55] T.Q. Trung, N.-E. Lee, Flexible and stretchable physical sensor integrated platforms for wearable human-activity monitoringand personal healthcare, Adv. Mater. 28 (2016) 4338–4372.
[56] J.L. Moore, J.E. Nordvik, A. Erichsen, I. Rosseland, E. Bø, T.G. Hornby, Implementation of high-intensity stepping training during inpatient stroke rehabilitation improves functional outcomes, Stroke 51 (2020) 563–570.